Effects of alloying elements (Al, Mn, Ru) on desorption plateau pressures of vanadium hydrides: an experimental and first-principles study

Zhiyang Liu[a,b,c], Liangyin Xiong[a], Jing Li[a], Shi Liu[a,*], Süleyman Er[c,d,*]

[a] *Institute of Metal Research, Chinese Academy of Sciences, 72 Wenhua Road, Shenyang, 110016, China*

[b] *School of Materials Science and Engineering, University of Science and Technology of China, 72 Wenhua Road, Shenyang, 110016, China*

[c] *DIFFER - Dutch Institute for Fundamental Energy Research, De Zaale 20, 5612 AJ Eindhoven, the Netherlands*

[d] *Center for Computational Energy Research, DIFFER - Dutch Institute for Fundamental Energy Research, De Zaale 20, 5612 AJ Eindhoven, the Netherlands*

* Corresponding author: s.er@differ.nl and sliu@imr.ac.cn

Abstract

Vanadium-based alloys are promising for the reversible, compressed storage of renewable hydrogen. To improve the hydrogen desorption plateau pressure of vanadium hydrides, V–3A binary alloys (i.e. $V_{97}Al_3$, $V_{97}Mn_3$, and $V_{97}Ru_3$) were prepared by vacuum arc melting. Hydrogen absorption and desorption properties of the newly prepared V–3A samples were studied, and compared to vanadium hydrides, by pressure-composition-temperature measurements and first-principles calculations. Among V–3A binary alloys, $V_{97}Ru_3$ achieved the highest hydrogen desorption plateau pressure while accommodating the highest atomic percentage of hydrogen. Meanwhile, it was also the alloy with the highest measured hardness.

Hydrogen desorption plateau pressures of V–3A alloys were complemented with DFT calculated formation energies. Calculated DOS, ELF and Bader charges showed that the influence of alloying on the electronic properties of the hydrides was comparable for Mn and Ru; whereas for Al alloying, vanadium dihydride bonding interactions were modified the most.

Keywords

vanadium hydrides; desorption plateau pressure; metal hydrides; hardness; density functional theory

1. Introduction

In recent years, the transition to renewable energy has attracted interest in developing efficient ways of producing and storing hydrogen [1]. For the latter, compressing of hydrogen using hydride forming metals, alloys or intermetallics offers a compact, safe, and reliable approach with simple design and operation principles [2]. Vanadium-based solid metallic compounds are interesting materials for reversible hydrogen storage with their fast hydrogen kinetics and steep temperature dependence of equilibrium pressure [3-6]. In a thermally driven vanadium hydride hydrogen compressor, hydrogen absorption takes place at low temperatures and accompanied with heat release as a result of an exothermic reaction between hydrogen and the body-centered cubic (*bcc*) structured host metal.

Incremental loading of vanadium with hydrogen results in vanadium hydrides with low, VH_{1-x}, and high, VH_{2-x}, hydrogen atomic percentages. Phase transition between the two hydrides is

reversible and shows a steep dependence of temperature to pressure and composition [7-9]. Hence, hydrogen desorption plateau pressures can be tuned through alloying and compositional variance, as has been shown in a number of studies [4, 10-17]. However, in these former studies, pressure-composition-temperature (PCT) isotherms were mostly collected at ambient temperature and the corresponding desorption pressures were not sufficient enough for high-pressure applications. Here, we studied, both experimentally and computationally, the effects of alloying elements, utilized in small amounts (~3 at. %), on the hydrogen desorption properties of vanadium hydrides. Al, Mn, and Ru were chosen as candidate-alloying elements at a relatively small atomic percentage to promote a *bcc* packing of metal solid solutions [11, 15-17]. The effects of alloying on the energetics and the electronic properties of the newly prepared hydrides were studied via PCT measurements and first-principles calculations.

2. Methods

2.1. Sample preparation

The alloy specimens used in the present investigation were ~ 25 g buttons that were prepared by vacuum arc melting method using high purity (>99.9%) elemental components with nominal composition of 3 mol%, i.e. V–3A alloys, where A= Al, Mn, and Ru. Contamination during arc melting was avoided by maintaining ultra-high purity inert atmosphere in the arc melting chamber. To ensure the homogeneity of new alloys, melting procedure was repeated a minimum of five times and the alloys were homogenized at 1373 K for 86.4 ks in a high purity argon gas atmosphere. Buttons were broken into pieces of approximately 1 mm in

thickness and were subsequently treated with acetone to remove oil, with 13% HNO_3 to remove surface oxide layers, and with 99% ethyl alcohol for a final cleaning.

2.2. Materials characterization

X-ray diffraction (XRD) data was measured using Bruker D8 ADVANCE X-ray diffractometer, within the 2θ region between 10° and 90° at a voltage of 40 kV and current of 40 mA. Uniformity of the prepared V–3A alloy samples was studied by Energy Dispersive X-ray Spectroscopy (EDS). Hardness of alloys was measured by Vickers indentation method, with a load of 9.8 N for 10 s. Newly prepared alloys were put into a modified Sieverts-type apparatus that achieved a maximum pressure of approximately 100 MPa for the activation of samples and the PCT measurements. The temperature sensor of the apparatus had a maximum measurement error of ±1 K while the pressure sensor had a maximum measurement error of 0.1% relative. The alloys were first activated at 773 K, in a vacuum of 1×10^{-3} Pa for 7.2 ks. Next, at room temperature, hydrogen gas at 6 MPa pressure was pumped into the apparatus. The activation procedure was repeated for three times for each sample. Hydrogen atomic content in alloys was calculated by using the van der Waals equation. When pressure is far from a standard atmospheric pressure, the influence of compression factor cannot be ignored. Therefore, we used a compression factor equation [18] that agrees with the National Institute of Standards and Technology (NIST) density data to within 0.01% from 220 K to 500 K with pressures from 0.1 MPa to 100 MPa. During hydrogen absorption and desorption processes, the changes in volumes of V–3A alloys were also taken into account.

2. 3. Computational methods

We carried out density functional theory (DFT) calculations to study the structure, energetics, and the electronic properties of the compounds in the present work. A plane wave basis and the projector augmented wave method (PAW) [19, 20] were employed as implemented in the Vienna *Ab Initio* Simulation Package (VASP) [21-23]. The plane-wave kinetic energy cut-off was set at 500 eV. Perdew−Burke−Ernzerhof (PBE) [24] functional was used as the generalized gradient approximation (GGA) to exchange and correlation. Brillouin zones were sampled using the Monkhorst−Pack scheme [25].

Metal alloys and their respective hydrides were treated using supercell geometries, whereas hydrogen molecule was calculated using a cubic box of 15 Å edge length. For the former, a *bcc* 2 × 2 × 4 supercell with a total of 32 metal atoms was used and sampled with a 12 × 12 × 6 **k**-point mesh. V–3A binary alloys were achieved by substituting a V atom with an alloying atom, A, where A = Al, Mn, and Ru.

To model the hydrides with low and high hydrogen content, 2 × 2 × 2 supercells of monoclinic V_2H with space group C2/m, and cubic VH and VH_2 both with space group $Fm\bar{3}m$ were constructed. The monoclinic and cubic supercells cells were sampled with **k**-point meshes of 6 × 9 × 6 and 6 × 6 × 6, respectively. Similar to alloys, to achieve 3 at. % metal alloying in the hydride phases, a V atom was substituted with an alloying element in the supercells that contained a total of 32 metal atoms. All the newly generated alloys and hydrides were fully optimized until the total forces acting on each atom were smaller than 0.01 eV/Å. The zero-point energy (ZPE), particularly for compounds that contain lightweight elements such as hydrogen, is not negligible [26-30]. Therefore, in addition to the formation

energy of the hydrides, here we also report the ZPE corrected formation energies.

3. Results and discussion

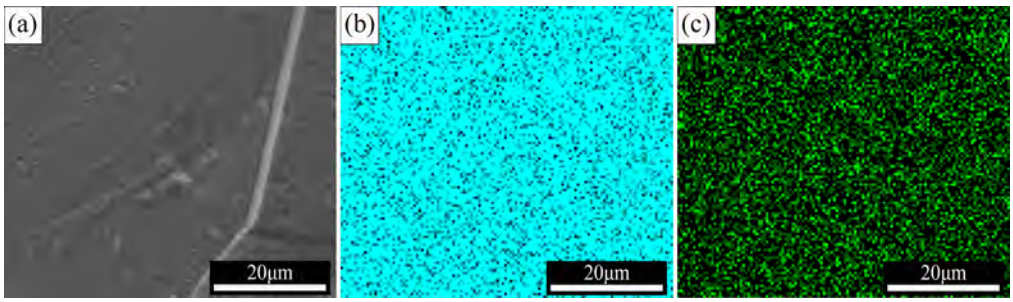

Figure 1. EDS element maps of V–3Ru with (a) the measured cross-section, (b, c) spatial distributions of V and Ru, respectively.

We first studied the structural features of the newly produced V–3A alloys. XRD results of V–3A (where A = V, Al, Mn, and Ru), as shown in Supporting Information (SI) Fig. S1, confirmed that all the compounds were solid solutions of their constituting elements with *bcc* structure. EDS was used to determine the spatial distribution of chemical elements within the alloy samples. Fig. 1 shows EDS produced element maps of a two dimensional cross-section through the V–3Ru alloy. Similar to V–3Ru, we found that all the other V–3A matrix alloys in our study were constituted of uniformly distributed elemental components.

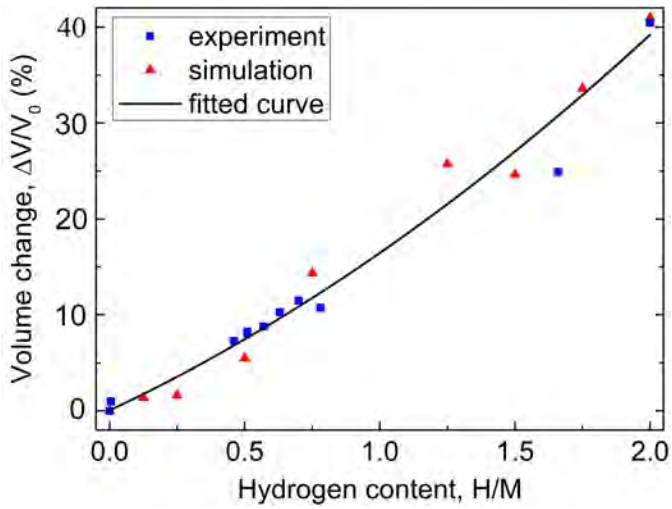

Figure 2. Volume change of vanadium hydrides as a result of hydrogen loading. Both experimental [31-35] (blue squares) and simulated [36] (red triangles) data were used to construct a curve (black line) with polynomial fitting.

All alloy samples were activated prior to PCT measurements. Alloying was found to improve the activation performance of V. Although pure V required activation twice, the newly prepared V–3A alloys were active after a single activation procedure. As the volume change of the alloys as a result of hydrogen loading and unloading was not negligible, the PCT measurements required metal alloy volumes to be rectified. For this purpose, we collected the volumes of the vanadium hydrides with different hydrogen loading ratios from literature and developed a fitting curve, as shown in Fig. 2, with

$$V_1 = V_0 + V_0 (0.132x + 0.032x^2) \quad (1)$$

where V_0 is the volume of the V–3A alloy preceding to hydrogen absorption, x and V_1 are the H/M atomic ratio and the volume of V–3A alloy proceeding to hydrogen absorption, respectively.

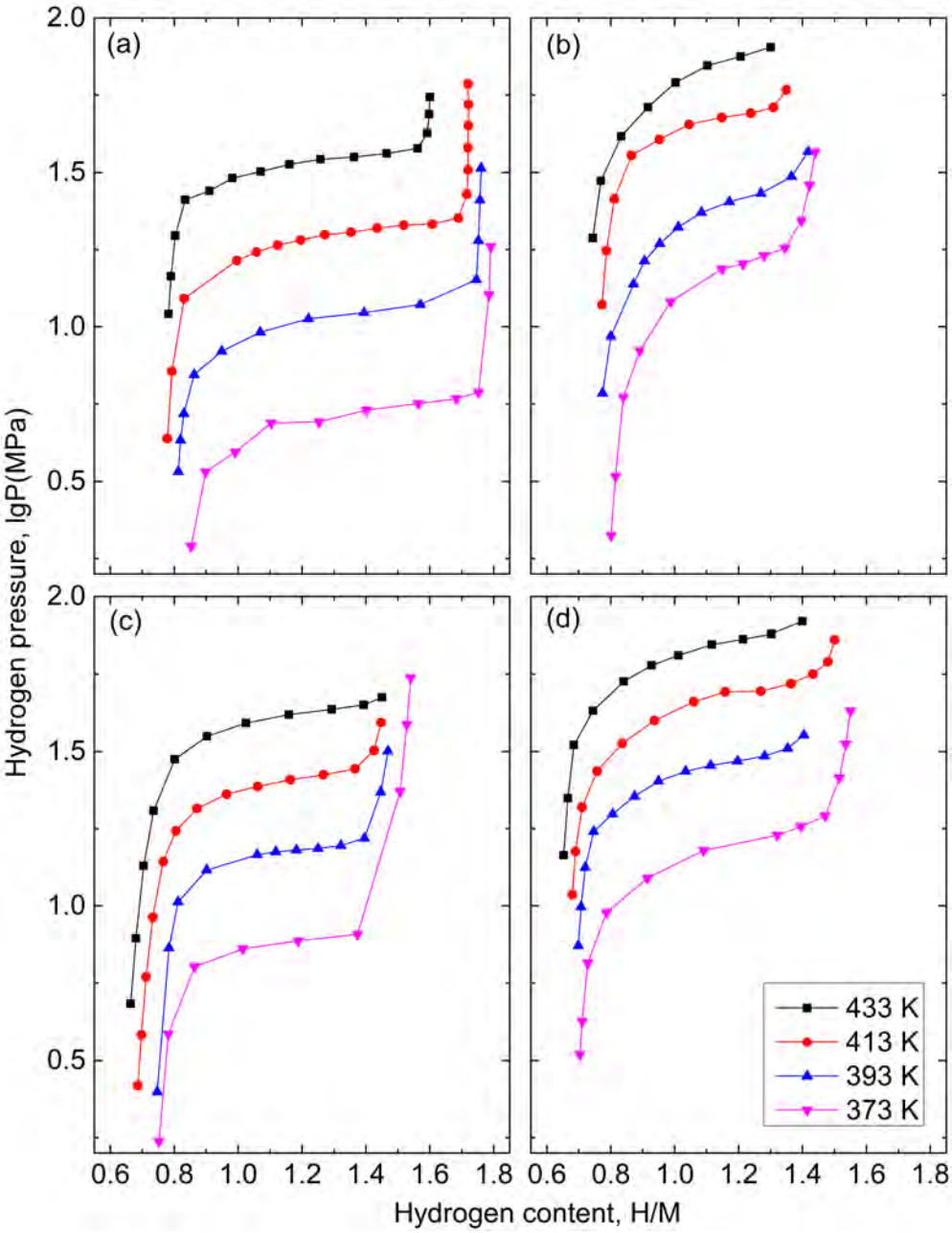

Figure 3. Desorption PCT curves of V–3A alloy hydrides, where A is (a) V, (b) Al, (c) Mn, and (d) Ru.

PCT isotherms of pure V and V–3A alloys are shown in Fig. 3. For each sample, the measurements were done between 373 and 433 K with 20 K intervals. The pressure value at the center of each plateau was referred to as the plateau pressure. As shown in Fig. 3(a), an increase in temperature was followed by an increase in hydrogen pressure, thereby indicating

a decrease in the total hydrogen content of vanadium hydride. This is also true for V–3A hydrides. However, Fig. 3(b-d) show that adding any of the alloying elements to vanadium matrix shifted the center of plateaus to the left and decreased the widths of plateaus. Among the hydrides, hydrogen desorption plateau widths were found to decrease in the following order: Ru < Mn < Al. Particularly for V–3Al, compressed hydrogen capacity of the alloy hydrides were significantly lower than pure V hydrides. Nevertheless, within the temperature range of our experiments, hydrogen desorption pressures of V–3A hydrides were all higher than that of pure V hydrides (see Fig. 4). For instance at T = 393 K, the measured plateau pressures of V, V–3Al, V–3Mn, and V–3Ru hydrides were 10.91, 25.85, 14.10, and 28.29 MPa, respectively (see Fig. S2).

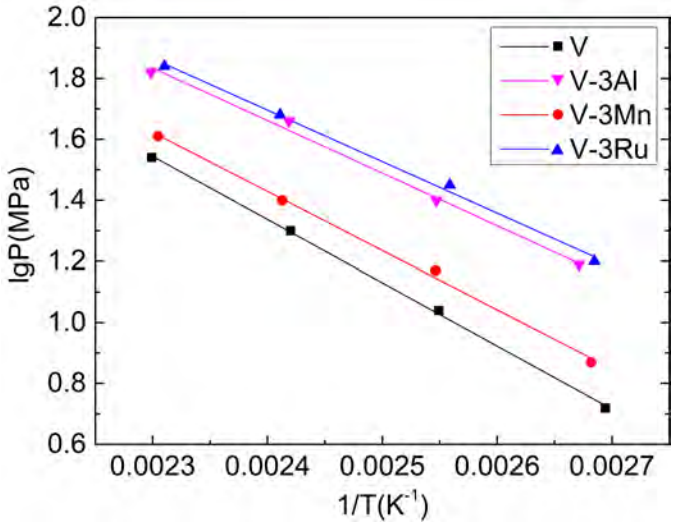

Figure 4. The van't Hoff plots of V–3A alloy hydrides, showing hydrogen desorption pressures and temperatures, obtained from data in Fig. 3.

	V	V–3Al	V–3Mn	V–3Ru
ΔH [kJ/(mol H_2)]	-39.63	-33.02	-37.08	-32.37
ΔS [J/(mol H_2 K)]	-120.71	-111.06	-116.35	-110.16

Table 1. Experimental values of the change in enthalpies (ΔH) and entropies (ΔS) for the V–3A hydrides.

Table 1 includes the experimental values of the enthalpy of hydride formation, ΔH, and the changes in entropy, ΔS, which were evaluated using the van't Hoff plots shown in Fig. 4. In our experiments, the enthalpy of VH_2 formation was -39.63 kJ/mol, which is in good agreement with the earlier reported results of -41.2 kJ/mol [3] and -40.26 kJ/mol [35]. For all the hydrides in our study, the changes in entropy during dehydrogenation were similar and the plateau pressures were determined mainly by ΔH. As shown in Table 1, all of the V–3A hydrides had ΔH values larger than that of pure vanadium hydride.

As shown in Fig. 2, during hydrogenation and dehydrogenation cycling of vanadium hydrides the materials experienced severe expansion and compression, respectively. If the residual stress during hydrogen cycling is difficult to accommodate, it may crack the alloy structure into smaller particles and pulverization occurs [37]. Considering a practical application of V-based alloys, pulverization cannot be ignored. To learn about the pulverization resistance of our V–3A alloys, we measured their Vickers Hardness [38]. Fig. 5 shows the measured values of hardness for our alloys as a bar graph. Adding Mn, Al and Ru into V matrix added on the hardness of compounds with an increasing order.

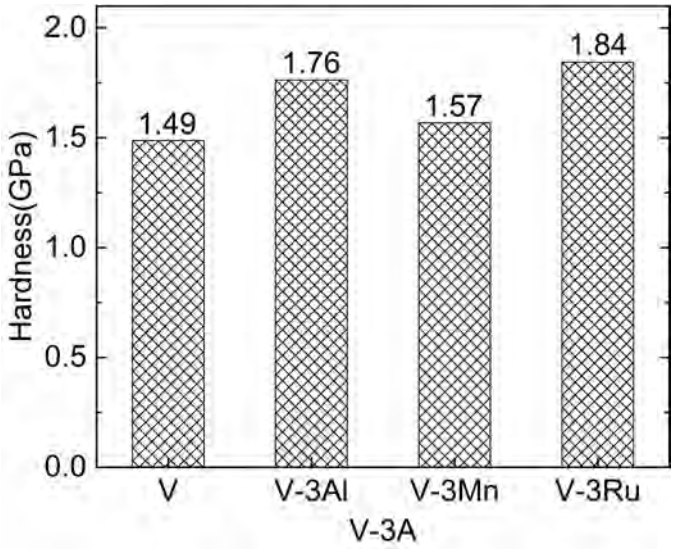

Figure 5. Vickers hardness of V–3A alloys.

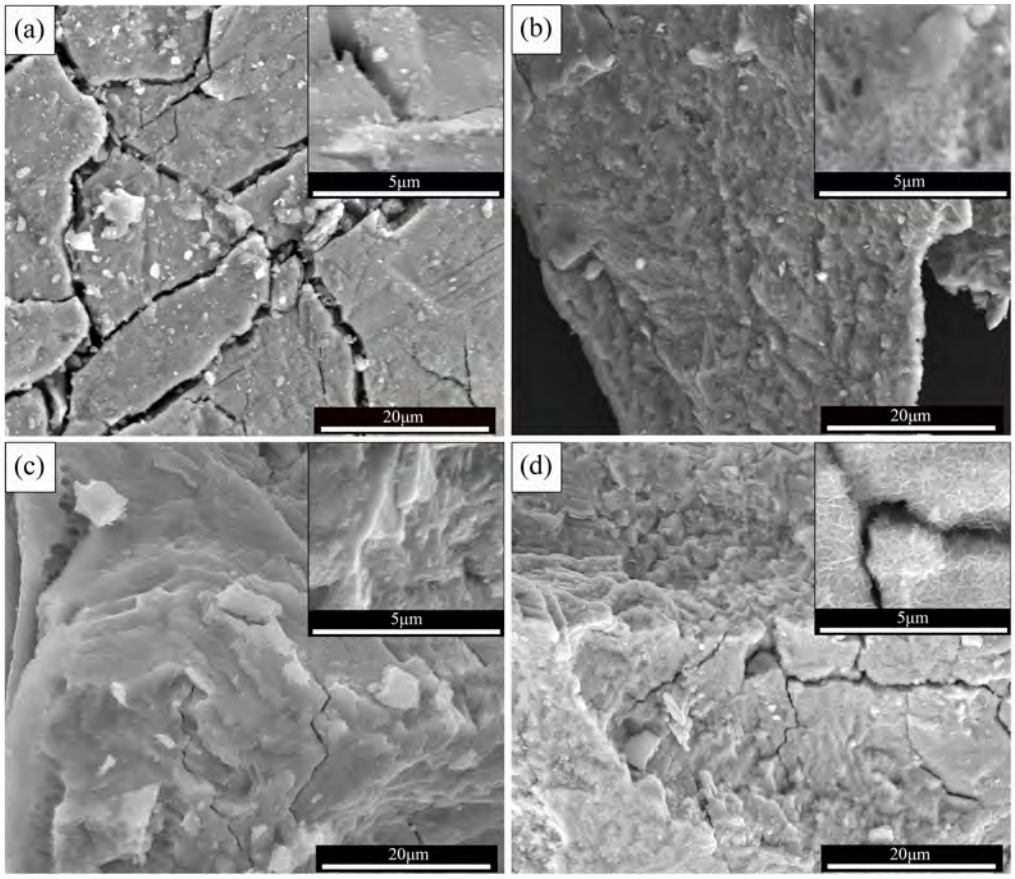

Figure 6. SEM micrographs of V–3A alloys after 20 hydrogen absorption/desorption cycles, where A is (a) V, (b) Al, (c) Mn, and (d) Ru.

Fig. 6 shows SEM measurements on V–3A compounds after 20 subsequent hydrogenation/dehydrogenation cycles. Visible cracks are apparent on the surfaces of all alloys. Particularly, the surface of V-3Ru has a whisker-like structure that would indicate a poor pulverization resistance, which is in line with our Vickers hardness measurements.

We performed DFT calculations to further investigate the effects of alloying on V compounds. First, we calculated the formation energies of alloys using a supercell approach. We used a 2 × 2 × 4 supercell of *bcc* crystal structure of V. To achieve an alloying composition as in our experiments, we substituted a single V atom with an atom of the alloying element, leading to approximately 3 at. % alloying element in the metal matrix. Alloy formation energies were calculated using

$$E_{\mathrm{Alloy}} = [E^{\mathrm{V-3A}} - (31E^{\mathrm{V}} + E^{\mathrm{A}})] / 32 \qquad (2)$$

where $E^{\mathrm{V-3A}}$, E^{V}, and E^{A} are DFT calculated total energies of 32 atom V–3A alloy supercells, per atom energies of pure vanadium and alloying elements in bulk form, respectively.

DFT calculated results confirmed the stability of V–3A alloys with respect to decomposition into their constituting metals. We found that Al, Mn, and Ru all form stable alloys with V, with alloy formation energies per atom (E_{Alloy}) of -0.018, -0.019, and -0.044 eV/atom, respectively. Inclusion of ZPE was found to have little effect on the metallic alloy formation energies. The ZPE corrected alloy formation energies per atom ($E_{\mathrm{Alloy}}^{\mathrm{ZPE}}$) at 0 K were calculated as -0.015, -0.017, and -0.041 eV/atom, for V–3Al, V–3Mn, and V–3Ru, respectively.

Next, we studied the energetics of metal hydride formation from the newly generated V–3A alloys and H_2 gas. We calculated the formation energy per metal (E_{Hyd}) of higher hydrides

(V–3A–H_h) from lower hydrides (V–3A–H_l), with $2 \geq h > l \geq 0$, using

$$E_{\mathrm{Hyd}} = E_h^{\mathrm{V-3A-H}} - [E_l^{\mathrm{V-3A-H}} + (\frac{h-l}{2}) E^{(\mathrm{H}_2)}] \quad (3)$$

where, $E_h^{\mathrm{V-3A-H}}$ and $E_l^{\mathrm{V-3A-H}}$ are the total energies of the hydrides per metal atom with high and low hydrogen content, respectively. Note that in the lower limit when *l* reaches zero, $E_l^{\mathrm{V-3A-H}}$ represents the total energy of V–3A alloy with no hydrogen inserted. $E^{(\mathrm{H}_2)}$ is the total energy of H_2 molecule in a 15 Å edge cubic box with periodicity. Table 2 shows the DFT calculated energies of hydride formation from V–3A metal alloys as well as from the lower hydrides.

The ZPE corrected hydride formation energies are also shown in Table 2. ZPE correction influenced the formation energies of hydrides more significantly than formation energies of V–3A alloys with no hydrogens. Because the atomic weight of hydrogen is small, its contribution to ZPE was significant [28, 39]. As shown in Fig. 7, for V–3A metal hydrides with equal hydrogen content, the ZPE contributions to the hydride formation energies were found to be similar, whereas increasing amount of hydrogen inside metal hydrides resulted in increasingly higher ZPE contributions. As a result, ZPE contributions were largest (i.e. ~0.2 eV/metal atom) when the formation energies of the fully hydrogenated hydrides are calculated directly from pure V–3A alloys. Clearly, alloying increased the hydride formation energy for all the phases of vanadium hydrides, as shown in Fig. 7. Particularly, the ZPE corrected formation energies for the fully hydrogenated V–3A alloys were in good agreement with our experimentally determined energies.

	From V to V_2H		From V_2H to VH		From V to VH		From VH to VH_2		From V_2H to VH_2		From V to VH_2	
	E_{Hyd}	$E_{\mathrm{Hyd}}^{\mathrm{ZPE}}$	E_{Hyd}	$E_{\mathrm{Hyd}}^{\mathrm{ZPE}}$	E_{Hyd}	$E_{\mathrm{Hyd}}^{\mathrm{ZPE}}$	E_{Hyd}	$E_{\mathrm{Hyd}}^{\mathrm{ZPE}}$	E_{Hyd}	$E_{\mathrm{Hyd}}^{\mathrm{ZPE}}$	E_{Hyd}	$E_{\mathrm{Hyd}}^{\mathrm{ZPE}}$
V	-0.20	-0.18	-0.09	-0.07	-0.30	-0.25	-0.30	-0.13	-0.39	-0.20	-0.59	-0.38
V–3Al	-0.18	-0.16	-0.09	-0.06	-0.27	-0.23	-0.24	-0.08	-0.33	-0.14	-0.51	-0.31
V–3Mn	-0.18	-0.17	-0.09	-0.06	-0.27	-0.23	-0.27	-0.11	-0.36	-0.17	-0.54	-0.33
V–3Ru	-0.17	-0.15	-0.08	-0.06	-0.26	-0.21	-0.25	-0.09	-0.34	-0.15	-0.51	-0.30

Table 2. DFT calculated formation energies, E_{Hyd} (eV/metal), of hydrides from the hydrogenation of metal alloys and lower hydrides. ZPE corrected formation energies, $E_{\mathrm{Hyd}}^{\mathrm{ZPE}}$ (eV/metal), are also provided.

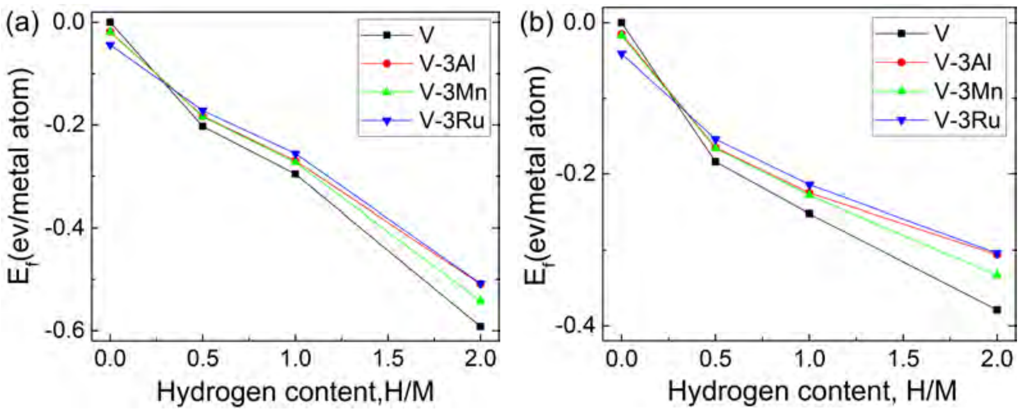

Figure 7. Calculated (a) formation energies and (b) ZPE corrected formation energies of V–3A alloys and hydrides. Data is from Table 2.

The calculated volume for *bcc* V bulk metal is 13.2 $Å^3$/metal atom. Volume changes were not significant for V–3A alloys, with 13.3, 13.1 and 13.2 $Å^3$/metal atom for Al, Mn, and Ru alloying, respectively. Hydrogenation increased the volumes of all the metal alloys, as shown in Fig. 8 and SI Table S1. The volumes of different V–3A hydrides with the same amounts of

hydrogen were within 1% of vanadium hydrides. Volumes of fully hydrogenated V–3A alloys increased approximately 41%, in very good agreement with the measurements shown in Fig. 2.

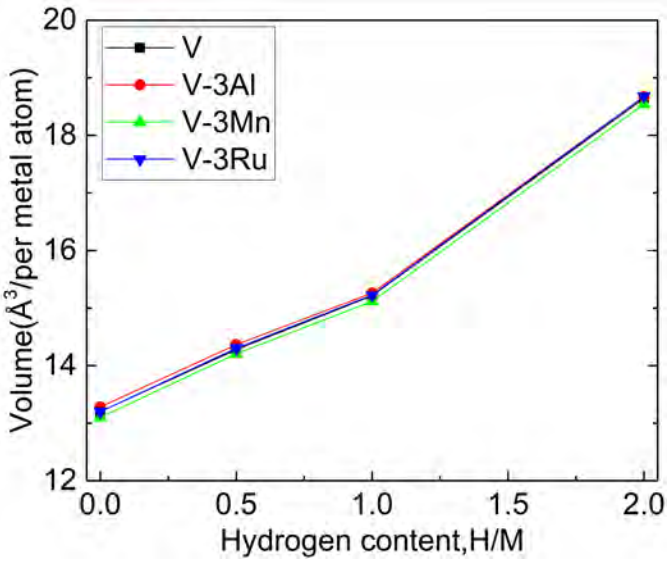

Figure 8. DFT optimized volumes of V–3A metal and hydride compounds.

To study the electronic structure of V–3A alloys upon hydrogenation, we calculated density of states (DOS) for the optimized structures of hydrides with increasing amounts of hydrogen. The DOS show similar features for different states of hydrogenation; therefore only the DOS for the fully hydrogenated compounds are shown here in Fig. 9, whereas the lower hydrides are included in SI Fig. S3 and S4. For all the hydrides, the DOS peaks at low energies, i.e. between -11 and -3 eV, resulted from bonding of hydrogens to the host metal atoms. These bonding interactions originated from the hybridization of H *s* electrons and the transition metal (V, Mn, and Ru) *p* and *d* electrons. As Al is missing d electrons, its interaction with nearby hydrogens operated through the *s* and *p* states of the metal. Around the zero energy,

transition metal *d* states dominated. At higher energies, the conduction states were populated with transition metal *d* states, Al *s* and p states, and H *s* states.

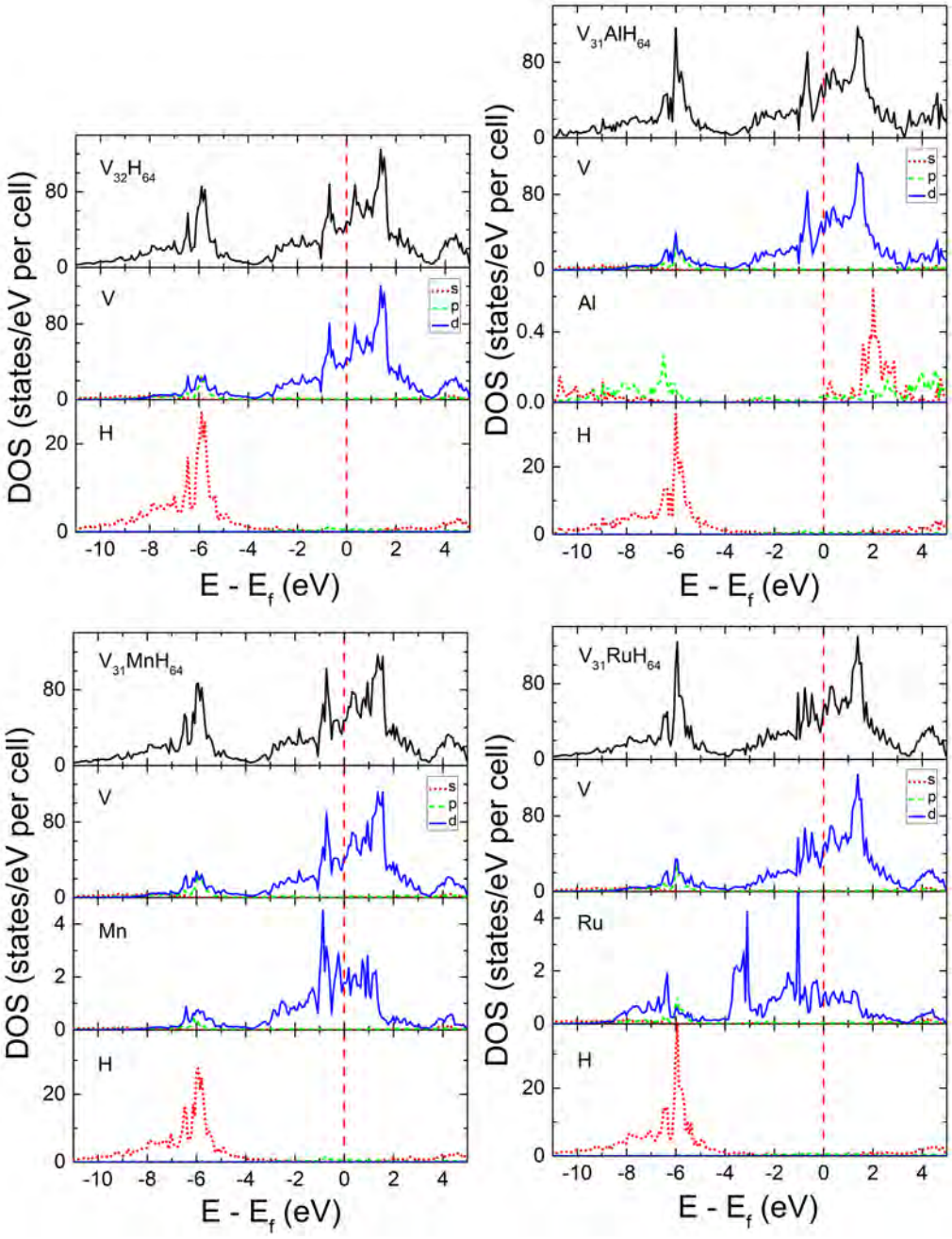

Figure 9. Densities of states of $V_{31}AH_{64}$, A = V, Mn, Al, and Ru. For each compound, the top figure is the total DOS, and the remaining figures represent the projected DOS on the atoms with *s, p* and *d* contributions shown in red, green and blue, respectively. The origin of energy

is set at the highest occupied state and indicated by a vertical dashed line.

We performed Bader charge analysis to obtain further information on bonding interactions in V–3A hydrides [40]. The calculated V atomic charges in compounds with formula units $MH_{0.5}$, MH, and MH_2 were +0.30, +0.64 and +1.00 *e*, respectively. Thus, in pure vanadium hydrides, V atoms were depleted more with an augmentation of absorbed hydrogens. The calculated Bader charges for Al in $V_{31}AlH_{16}$, $V_{31}AlH_{32}$, and $V_{31}AlH_{64}$ were +0.27, +0.94, and +2.30 *e*, respectively. For Mn in $V_{31}MnH_{16}$, $V_{31}MnH_{32}$, and $V_{31}MnH_{64}$, Bader charges were -0.47, +0.16, and +0.63 *e*, respectively. The charges on Ru atoms in $V_{31}RuH_{16}$, $V_{31}RuH_{32}$, and $V_{31}RuH_{64}$ were -1.05, -0.47, and +0.25 *e*, respectively. Interestingly, in contrary to V and Al, both Mn and Ru were charged negatively in lower V–3A hydrides, but they became positively charged in higher hydrides. Fig. 10 shows Bader charges of atoms in V–3A alloys in their fully hydrogenated states, $V_{31}AH_{64}$. In the pure vanadium dihydride (Fig. 10(a)), the charges on H atoms were half of charges on V atoms but with opposite sign. As shown in Fig. 10(b), alloying with Al created charge inhomogeneity within the whole compound and when compared to pure vanadium dihydride it resulted in a larger charge transfer to the first neighbor hydrogen atoms of Al. In Mn and Ru alloyed vanadium dihydrides, as shown in Fig. 10(c) and (d), Bader charges on eight of hydrogen atoms that were first order neighbors to the alloying element were slightly different than the remainder of hydrogens in these materials. In all of the alloyed dihydrides, the calculated Bader charges on V atoms were within 0.1 *e* of each other. Further details of charge analysis for the different hydride compositions are provided in SI Tables S2-S4.

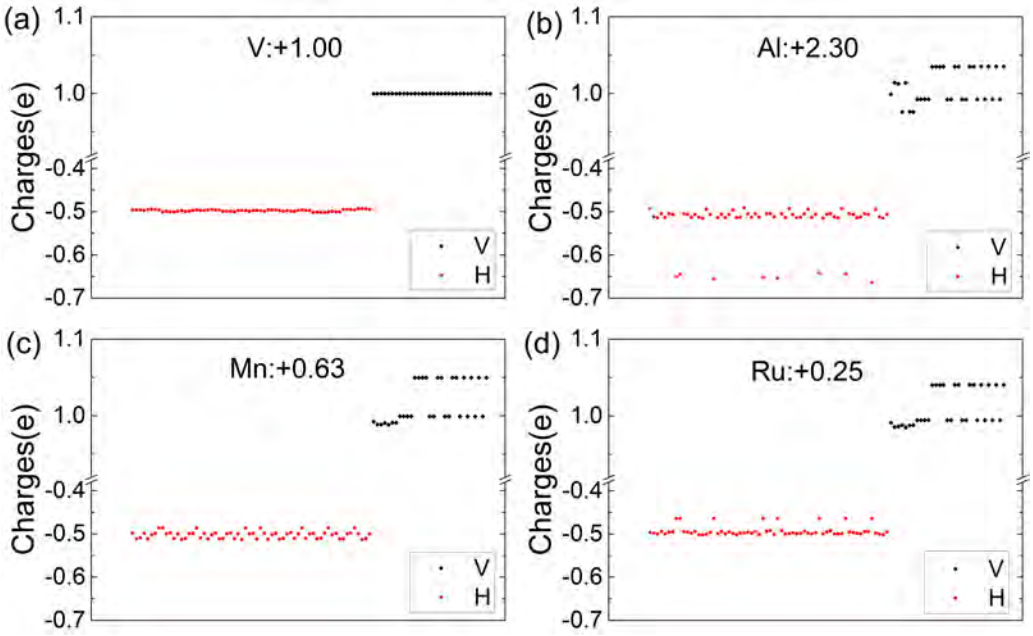

Figure 10. Bader charge analysis of $V_{31}AH_{64}$, where A is (a) V, (b) Al, (c) Mn, and (d) Ru. All charges are given in units of *e*.

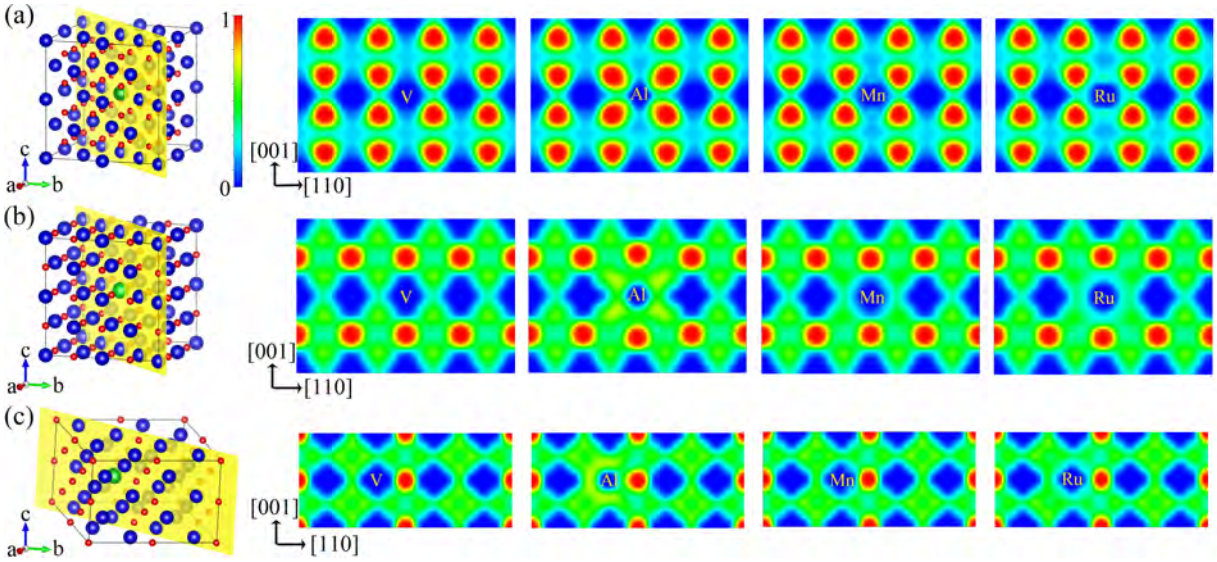

Figure 11. ELFs for (a) $V_{31}AH_{64}$, (b) $V_{31}AH_{32}$, (c) $V_{31}AH_{16}$, where from left to right, A = V, Al, Mn, and Ru, respectively. In representative structures for different compositions, shown on left, V, H, and the alloying elements are colored as blue, red, and green spheres, respectively. Cut-planes for ELF analysis are also shown as yellow shaded areas in the

hydride structures.

Fig. 11, from (a) to (c), shows the Electron Localization Function (ELF) for the V–3A hydrides with decreasing number of hydrogen atoms per formula unit. For all the hydride compounds, ELF was maximized around H atoms, indicating electron localization, and it was minimized around V atoms due to electron depletion. Additionally, ionicity in bonding increased with increasing amount of hydrogen inserted into the metal alloys. These findings are in line with our Bader and DOS analyses.

4. Conclusions

We studied the influence of using small amount (3 at. %) of alloying elements (Al, Mn, and Ru) on the high-pressure plateau of vanadium hydrides. Conducting PCT measurements we found that insertion of any of these elements into vanadium subsequently increased hydrogen desorption pressures at high temperatures. In line with this finding, our computational predictions confirmed that addition of these elements slightly destabilized hydride phases with high hydrogen content, whereas the effects of alloying on lower hydrides were limited. Nevertheless, the effective hydrogen absorption amounts in all alloyed samples were lower than that in vanadium hydrides. Among the alloys, V–3Ru achieved the maximum effective hydrogen absorption and the highest hydrogen release plateau pressure. However, within the group of V–3A alloys, Ru alloyed samples also had the highest hardness, therefore were prone to pulverization the most. According to our Bader charge analysis, DOS and ELF calculations, hydrides of V–3Al showed different electronic properties when compared to

hydrides alloyed with transition metals, i.e. V–3Mn and V–3Ru.

Acknowledgements

We gratefully acknowledge funding by The Dutch Organisation for Internationalization in Education (NUFFIC) and the China Scholarship Council (CSC) for enabling ZL to perform his studies at DIFFER. SE acknowledges funding from the initiative "Computational Sciences for Energy Research' of Shell and the Netherlands Organisation for Scientific Research (NWO). Computational work was carried out on the Dutch national e-infrastructure with the support of SURF Cooperative.

Declaration of interest:

None.

References

[1] Coontz R, Hanson B. Not so simple. Science. 2004;305:957. https://doi.org/10.1126/science.305.5686.957

[2] Stamatakis E, Zoulias E, Tzamalis G, Massina Z, Analytis V, Christodoulou C, et al. Metal hydride hydrogen compressors: Current developments & early markets. Renewable Energy. 2018;127:850-62. . https://doi.org/10.1016/j.renene.2018.04.073

[3] Golubkov A, Yukhimchuk A. High-pressure hydrogen isotopes sources based on vanadium hydride. Hyperfine Interactions. 2001;138:403-8. https://doi.org/10.1023/A:1020854007760

[4] Lototskyy M, Yartys V, Pollet B, Bowman R. Metal hydride hydrogen compressors: a review. International Journal of Hydrogen Energy. 2014;39:5818-51. https://doi.org/10.1016/j.ijhydene.2014.01.158

[5] Bowman Jr R, Freeman B, Phillips J. Evaluation of metal hydride compressors for applications in Joule-Thomson cryocoolers. Cryogenics. 1992;32:127-37. https://doi.org/10.1016/0011-2275(92)90255-9

[6] Selvaraj S, Jain A, Kumar S, Zhang T, Isobe S, Miyaoka H, et al. Study of cyclic performance of V-Ti-Cr alloys employed for hydrogen compressor. International Journal of Hydrogen Energy. 2018;43:2881-9. https://doi.org/10.1016/j.ijhydene.2017.12.159

[7] Kumar S, Tiwari G, Krishnamurthy N. Tailoring the hydrogen desorption thermodynamics of V2H by alloying additives. Journal of Alloys and Compounds. 2015;645:S252-S6. https://doi.org/10.1016/j.jallcom.2014.12.246

[8] Lamb J, Chandra D, Coleman M, Sharma A, Cathey WN, Paglieri SN, et al. Low and high-pressure hydriding of

V–0.5 at.% C. Journal of Nuclear Materials. 2010;399:55-61. https://doi.org/10.1016/j.jnucmat.2010.01.002
[9] Yukawa H, Yamashita D, Ito S, Morinaga M, Yamaguchi S. Compositional dependence of hydriding properties of vanadium alloys at low hydrogen pressures. Journal of Alloys and Compounds. 2003;356:45-9. https://doi.org/10.1016/S0925-8388(03)00099-9
[10] Kumar S, Jain A, Ichikawa T, Kojima Y, Dey G. Development of vanadium based hydrogen storage material: a review. Renewable and Sustainable Energy Reviews. 2017;72:791-800. https://doi.org/10.1016/j.rser.2017.01.063
[11] Yukawa H, Takagi M, Teshima A, Morinaga M. Alloying effects on the stability of vanadium hydrides. Journal of Alloys and Compounds. 2002;330:105-9. https://doi.org/10.1016/S0925-8388(01)01526-2
[12] Lototsky M, Yartys V, Zavaliy IY. Vanadium-based BCC alloys: phase-structural characteristics and hydrogen sorption properties. Journal of Alloys and Compounds. 2005;404:421-6. https://doi.org/10.1016/j.jallcom.2005.01.139
[13] Lynch J, Reilly J, Millot F. The absorption of hydrogen by binary vanadium-chromium alloys. Journal of Physics and Chemistry of Solids. 1978;39:883-90. https://doi.org/10.1016/0022-3697(78)90150-6
[14] Verbetsky V, Zotov T, Movlaev E. Absorption of hydrogen by V-Mo and V-Mo-Ti alloys. Inorganic Materials: Applied Research. 2014;5:70-4. https://doi.org/10.1134/S2075113314010134
[15] Kumar S. Studies on hydrogen interaction with vanadium and vanadium-aluminum alloys [PhD thesis]. Mumbai, India: Homi Bhabha National Institute; 2012.
[16] Seo C-Y, Kim J-H, Lee PS, Lee J-Y. Hydrogen storage properties of vanadium-based bcc solid solution metal hydrides. Journal of Alloys and Compounds. 2003;348:252-7. https://doi.org/10.1016/S0925-8388(02)00831-9
[17] Tominaga Y, Matsumoto K, Fuda T, Tamura T, Kuriiwa T, Kamegawa A, et al. Protium absorption-desorption properties of Ti–V–Cr–(Mn, Ni) alloys. Materials Transactions, JIM. 2000;41:617-20. https://doi.org/10.2320/matertrans1989.41.617
[18] Zheng J, Zhang X, Xu P, Gu C, Wu B, Hou Y. Standardized equation for hydrogen gas compressibility factor for fuel consumption applications. International Journal of Hydrogen Energy. 2016;41:6610-7. https://doi.org/10.1016/j.ijhydene.2016.03.004
[19] Blöchl PE. Projector augmented-wave method. Physical Review B. 1994;50:17953. https://doi.org/10.1103/PhysRevB.50.17953
[20] Kresse G, Joubert D. From ultrasoft pseudopotentials to the projector augmented-wave method. Physical Review B. 1999;59:1758. https://doi.org/10.1103/PhysRevB.59.1758
[21] Kresse G, Hafner J. Ab initio molecular dynamics for open-shell transition metals. Physical Review B. 1993;48:13115. https://doi.org/10.1103/PhysRevB.48.13115
[22] Kresse G, Furthmüller J. Efficiency of ab-initio total energy calculations for metals and semiconductors using a plane-wave basis set. Computational Materials Science. 1996;6:15-50. https://doi.org/10.1016/0927-0256(96)00008-0
[23] Kresse G, Furthmüller J. Efficient iterative schemes for ab initio total-energy calculations using a plane-wave basis set. Physical Review B. 1996;54:11169. https://doi.org/10.1103/PhysRevB.54.11169
[24] Perdew JP, Burke K, Ernzerhof M. Generalized gradient approximation made simple. Physical Review Letters. 1996;77:3865. https://doi.org/10.1103/PhysRevLett.77.3865
[25] Monkhorst HJ, Pack JD. Special points for Brillouin-zone integrations. Physical Review B. 1976;13:5188. https://doi.org/10.1103/PhysRevB.13.5188
[26] Miwa K, Ohba N, Towata S-i, Nakamori Y, Orimo S-i. First-principles study on lithium borohydride $LiBH_4$. Physical Review B. 2004;69:245120. https://doi.org/10.1103/PhysRevB.69.245120
[27] Kamakoti P, Sholl DS. A comparison of hydrogen diffusivities in Pd and CuPd alloys using density functional

theory. Journal of Membrane Science. 2003;225:145-54. https://doi.org/10.1016/j.memsci.2003.07.008
[28] Bourgeois N, Crivello J-C, Cenedese P, Joubert J-M. Systematic First-Principles Study of Binary Metal Hydrides. ACS Combinatorial Science. 2017;19:513-23. https://doi.org/10.1021/acscombsci.7b00050
[29] Ouyang C, Lee Y-S. Hydrogen-induced interactions in vanadium from first-principles calculations. Physical Review B. 2011;83:045111. https://doi.org/10.1103/PhysRevB.83.045111
[30] Frankcombe TJ. The importance of vibrations in modelling complex metal hydrides. Journal of Alloys and Compounds. 2007;446:455-8. https://doi.org/10.1016/j.jallcom.2007.01.050
[31] Maeland AJ, Gibb Jr TR, Schumacher DP. A NOVEL HYDRIDE OF VANADIUM[1]. Journal of the American Chemical Society. 1961;83:3728-9. https://doi.org/10.1021/ja01478a047
[32] Maeland AJ. Investigation of the vanadium-hydrogen system by x-ray diffraction techniques[1, 2]. The Journal of Physical Chemistry. 1964;68:2197-200. https://doi.org/10.1021/j100790a028
[33] Asano H, Hirabayashi M. Low-temperature phase transition near V_3H_2. Physica Status Solidi (a). 1973;16:69-72. https://doi.org/10.1002/pssa.2210160106
[34] Golubkov A, Gudarenko L, Zhernokletov M, Kayakin A, Shuikin A. Shock compression of vanadium hydrides and deuterides with different concentrations of gas atoms. Combustion, Explosion, and Shock Waves. 2017;53:309-18. https://doi.org/10.1134/S001050821703008X
[35] Reilly JJ, Wiswall RH. Higher hydrides of vanadium and niobium. Inorganic Chemistry. 1970;9:1678-82. https://doi.org/10.1021/ic50089a013
[36] Peng S, Zhao P, Yang M, Yao S, Luo S, Xu Z. Simulation on crystal structures of metallic V and its hydrides. Atomic Energy Science and Technology. 2000;34:469-72.
[37] Miao H, Wang WG. Mechanisms of improving the cyclic stability of V–Ti-based hydrogen storage electrode alloys. Journal of Alloys and Compounds. 2010;508:592-8. https://doi.org/10.1016/j.jallcom.2010.08.132
[38] Tsukahara M, Takahashi K, Mishima T, Isomura A, Sakai T. Vanadium-based solid solution alloys with three-dimensional network structure for high capacity metal hydride electrodes. Journal of Alloys and Compounds. 1997;253:583-6 . https://doi.org/10.1016/S0925-8388(96)02912-X
[39] Er S, Tiwari D, de Wijs GA, Brocks G. Tunable hydrogen storage in magnesium–transition metal compounds: First-principles calculations. Physical Review B. 2009;79:024105. https://doi.org/10.1103/PhysRevB.79.024105
[40] Henkelman G, Arnaldsson A, Jónsson H. A fast and robust algorithm for Bader decomposition of charge density. Computational Materials Science. 2006;36:354-60. https://doi.org/10.1016/j.commatsci.2005.04.010